JOURNAL OF GUIDANCE, CONTROL, AND DYNAMICS
Vol. 34, No. 4, July–August 2011

Vibration Control Using Input Shaping and Adaptive Positive Position Feedback

Ryan R. Orszulik* and Jinjun Shan†
York University, Toronto, Ontario M3J 1P3, Canada

DOI: 10.2514/1.52287

This paper presents a vibration control strategy for a flexible manipulator with a collocated piezoelectric sensor/actuator pair. Dynamic modeling of the flexible manipulator is first shown, and then a control law is developed. The proposed vibration controller combines the input shaping technique with multimode adaptive positive position feedback. An adaptive parameter estimator based on the recursive least-square method is developed to update the system's natural frequencies, which are used by the adaptive positive position feedback. A proportional-derivative controller is combined with the proposed vibration controller to suppress vibration while slewing the manipulator. Simulation results are presented to illustrate the efficacy of the proposed controller.

I. Introduction

FLEXIBLE manipulator systems exhibit many advantages over their rigid counterparts. They possess a higher load ratio, and a large increase in the speed of the links is possible. They require less power to produce the same acceleration as the rigid links which have the same load carrying capacity, hence inexpensive and smaller actuators are sufficient. Because of the high performance requirements, consideration of structural flexibility in robots arms is a real challenge. Unfortunately, taking into account the flexibility of the arm leads to the appearance of oscillations at the tips of the links during the motion. These oscillations make the control problems of such systems very difficult. There has been extensive research on active vibration control of flexible systems (see, e.g., [1]). Many control strategies have been used in the control of lightweight flexible structures. These control strategies include, but are not limited to: adaptive control [2], fuzzy logic control [3], H_∞ control [4], and time-optimal control [5].

With the developments in sensor/actuator technologies, many researchers have concentrated on vibration control using smart materials such as shape memory alloys and piezoelectric transducers, among others. Piezoelectric materials have been applied in structural vibration control as well as in structural acoustics because of their advantages of fast response, large force output and the fact that they generate no magnetic field in the conversion of electrical energy into mechanical motion. Positive position feedback (PPF) was devised by Goh and Caughey [6] and has several distinguished advantages [7]. It has been shown to be a solid vibration control strategy for flexible systems with smart materials, particularly with the PZT (lead zirconium titanate) type of piezoelectric material [7–10]. PPF is essentially a second-order filter that is used to apply high frequency gain stabilization by improving the frequency rolloff of the system [11]. Alternatively, PPF works by using a second-order system which is forced by the position response of the structure. This response is then fed back to give the force input to the structure. To apply PPF, the natural frequencies of the structure should be known. The effectiveness of PPF will deteriorate when the natural frequencies are poorly known or have changed due to, for example, the presence of a tip mass.

One of the most successful methods used to control flexible structures is that of input shaping. Figure 1 shows the process of input shaping. With this method, a command is convolved with a sequence of impulses, called an input shaper, to produce a shaped command that causes less vibration than the original unshaped command [12]. The earliest work on input shaping (or command shaping) was conducted by O. J. M. Smith in the late 1950s [13]. The posicast method proposed by Smith effectively took two impulses whose vibrations were self-canceling and convolved them with the baseline reference command. Because of its sensitivity to frequency uncertainty, the input shaping method was not widely used until robust methods were developed by Singer and Seering in [12]. So far, more than 700 papers on this subject have been published [14] and input shaping has been implemented on a variety of systems, such as large space-based antenna [15], long-reach manipulator [16], crane [17], flexible manipulator [18,19], and flexible spacecraft [20–26].

There are various versions of the input shaping control technique, such as zero-vibration (ZV) shaper [12], zero-vibration-derivative (ZVD) shaper [12], zero-vibration-derivative-derivative (ZVDD) shaper [12], specified-insensitivity shaper [27], and extra-insensitive shaper [22,28]. These input shapers can suppress residual vibrations if the system parameters are well known, or the change in modeling parameters is limited to within a reasonable bound. However, if the system has a large range of unknown or varying frequencies, then another approach is needed to make the control methods more robust [29].

One approach is to use adaptive input shaping techniques. Tzes and Yurkovich have proposed online adaptive schemes to update the input shaper parameters [30]. Bodson has used a recursive least-squares technique to tune the input shaper parameters [31]. Kojima and Singhose have proposed an adaptive deflection-limiting input shaping control for slewing flexible space structures [29].

This paper presents a new approach to overcome the problem of large parameter uncertainties. Rather than using adaptive input shaping techniques, a control strategy is proposed here to combine the input shaping with a multimode adaptive PPF in order to suppress the flexible vibration while slewing the flexible system. Input shaping is used to shape the command in order to minimize the flexible vibration induced by the maneuver. Any residual vibrations will be suppressed by the PZT actuator and the proposed multimode adaptive PPF. Hu and Ma combined input shaping with PPF and showed good results for vibration control of a flexible spacecraft [25]. However, for this control method to be effective, the frequencies must be known accurately. A few forms of adaptive PPF have been developed for constrained stuctures in [32–34], which vary in the way they are implemented. In this paper, input shaping is combined with multimode adaptive PPF to suppress the vibrations of a slewing flexible manipulator with frequency uncertainty.

Presented as Paper 2010-8147 at the AIAA Guidance, Navigation, and Control Conference, Toronto, Canada, 2–5 August 2010; received 24 September 2010; revision received 12 November 2010; accepted for publication 1 December 2010.

*Ph.D. Candidate, Department of Earth and Space Science and Engineering, 4700 Keele Street; orszulik@yorku.ca. Student Member AIAA.

†Assistant Professor, Department of Earth and Space Science and Engineering, 4700 Keele Street; jjshan@yorku.ca. Senior Member AIAA.

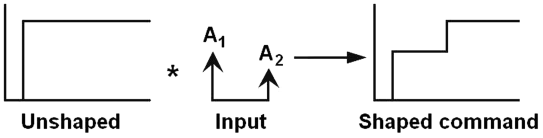

Fig. 1 Principle of input shaping.

The organization of the paper is as follows. Section II describes the dynamic modeling of a flexible manipulator with bonded piezoelectric sensors and actuators using the finite element method. The flexible manipulator without piezoelectric elements is modeled first, then the effects of the piezoelectric sensor/actuator are taken into account. In Sec. III, an active vibration control system is designed by combining the input shaping technique and multimode adaptive PPF. In Sec. IV, the results of simulation and their discussion are given. Section V presents the conclusions.

II. Dynamic Modeling

Figure 2 shows the diagram of the flexible manipulator being modeled. The flexible manipulator system consists of a rigid hub, a flexible beam, a tip mass, and a collocated piezoelectric sensor/actuator pair. In this study, the flexible manipulator without the piezoelectric sensor/actuator pair will be modeled first using the finite element method and the dynamics equations will be augmented later to consider the effects of the piezoelectric sensor/actuator pair.

The kinetic energy of the system assuming an Euler–Bernoulli beam is [35]

$$T = \frac{1}{2} I_h \dot{\theta}^2 + \frac{1}{2}\int_0^L \rho A[\dot{w} + (b+x)\dot{\theta}]^2\,\mathrm{d}x + \frac{1}{2} m_{\text{tip}}[(b+L)\dot{\theta} + \dot{w}(L,t)]^2 + \frac{1}{2} I_{\text{tip}}[\dot{\theta} + \dot{w}'(L,t)]^2 \tag{1}$$

where the first term is due to the rigid hub, the second term is due to the energy of the beam with respect to its velocity normal to x, the third term is due to the tip mass, and the last term is due to the inertia of the tip mass.

The potential energy of the system remains the same as that for a simple beam due to the fact that a rigid body will make no contribution to this term.

It can be seen that after discretizing the body into elements, the first element will have kinetic energy expression given by

$$T_1 = \frac{1}{2} I_h \dot{\theta}^2 + \frac{1}{2}\int_0^l \rho A[\dot{w} + (b + x + x_i)\dot{\theta}]^2\,\mathrm{d}x \tag{2}$$

where l is the length of the element. The ith element, where $i = 2$ to $n-1$, will have kinetic energy:

$$T_i = \frac{1}{2}\int_0^l \rho A[\dot{w} + (b + x + x_i)\dot{\theta}]^2\,\mathrm{d}x \tag{3}$$

where x_i is the distance from the root of the beam to the closest side of the ith beam element. The last element of the beam will have kinetic energy:

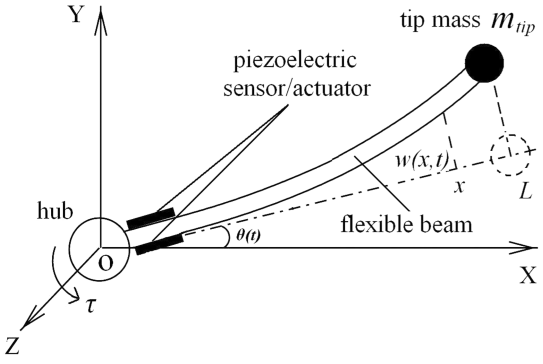

Fig. 2 Diagram of flexible manipulator.

$$T_n = \frac{1}{2}\int_0^l \rho A[\dot{w} + (b + x + x_i)\dot{\theta}]^2\,\mathrm{d}x + \frac{1}{2} m_{\text{tip}}[(b+L)\dot{\theta} + \dot{w}(L,t)]^2 + \frac{1}{2} I_{\text{tip}}[\dot{\theta} + \dot{w}'(L,t)]^2 \tag{4}$$

This naturally leads to an augmentation of the traditional Euler–Bernoulli finite element shape functions to

$$[N]^T = \begin{bmatrix} (b + x_i + x) \\ 1 - 3\left(\frac{x}{l}\right)^2 + 2\left(\frac{x}{l}\right)^3 \\ \frac{x}{l} - 2\left(\frac{x}{l}\right)^2 + \left(\frac{x}{l}\right)^3 \\ 3\left(\frac{x}{l}\right)^2 - 2\left(\frac{x}{l}\right)^3 \\ -\left(\frac{x}{l}\right)^2 + \left(\frac{x}{l}\right)^3 \end{bmatrix} \tag{5}$$

While strictly speaking, x_i is a variable in the global sense, it can be treated simply as a constant in the local coordinate system of the elements as it is simply a length offset, which allows the shape functions to be augmented as described previously.

The mass matrix of each element can then be seen as [35]

$$[M^e] = \rho A \int_0^l [N]^T[N]\,\mathrm{d}x = \begin{bmatrix} M^e_{\theta\theta} & M^e_{\theta w} \\ M^{eT}_{\theta w} & M^e_{ww} \end{bmatrix} \tag{6}$$

where

$$M^e_{\theta\theta} = \frac{\rho A l}{3}[(x_i+b)^2 + (x_i+b+l)(x_i+b) + (x_i+b+l)^2] \tag{7}$$

$$M^e_{\theta w} = \rho A l \begin{bmatrix} \frac{3}{20}l + \frac{1}{2}(x_i+b) \\ \frac{1}{30}l^2 + \frac{1}{12}l(x_i+b) \\ \frac{7}{20}l + \frac{1}{2}(x_i+b) \\ -\frac{1}{20}l^2 - \frac{1}{12}l(x_i+b) \end{bmatrix}^T \tag{8}$$

$$M^e_{ww} = \frac{\rho A l}{420}\begin{bmatrix} 156 & 22l & 54 & -13l \\ 22l & 4l^2 & 13l & -3l^2 \\ 54 & 13l & 156 & -22l \\ -13l & -3l^2 & -22l & 4l^2 \end{bmatrix} \tag{9}$$

As indicated in the kinetic energy expression for the first element, there will be a contribution from the inertia of the rigid hub, thus for the first element $M^e_{\theta\theta}$ becomes

$$M^e_{\theta\theta} = I_h + \frac{\rho A l}{3}[(x_i+b)^2 + (x_i+b+l)(x_i+b) + (x_i+b+l)^2] \tag{10}$$

Similarly, for the last element, there will be a contribution from the mass and inertia of the tip mass, thus for the last element $M^e_{\theta w}$ and M^e_{ww} become

$$M^n_{\theta w} = M^e_{\theta w} + M^e_{\theta t} = \rho A l \begin{bmatrix} \frac{3}{20}l + \frac{1}{2}(x_i+b) \\ \frac{1}{30}l^2 + \frac{1}{12}l(x_i+b) \\ \frac{7}{20}l + \frac{1}{2}(x_i+b) \\ -\frac{1}{20}l^2 - \frac{1}{12}l(x_i+b) \end{bmatrix}^T + \begin{bmatrix} 0 \\ 0 \\ m_{\text{tip}}(b+L) \\ I_{\text{tip}} \end{bmatrix}^T \tag{11}$$

$$M^n_{ww} = M^e_{ww} + M_{wt} = \frac{\rho A l}{420}\begin{bmatrix} 156 & 22l & 54 & -13l \\ 22l & 4l^2 & 13l & -3l^2 \\ 54 & 13l & 156 & -22l \\ -13l & -3l^2 & -22l & 4l^2 \end{bmatrix} + \begin{bmatrix} 0 & 0 & 0 & 0 \\ 0 & 0 & 0 & 0 \\ 0 & 0 & m_{\text{tip}} & 0 \\ 0 & 0 & 0 & I_{\text{tip}} \end{bmatrix} \tag{12}$$

Taking the second spatial derivative of the shape function matrix $[N]$ gives

$$[B]^T = \begin{bmatrix} 0 \\ \frac{1}{l^2}\left[-6 + 12\left(\frac{x}{l}\right)\right] \\ \frac{1}{l}\left[-4 + 6\left(\frac{x}{l}\right)\right] \\ \frac{1}{l^2}\left[6 - 12\left(\frac{x}{l}\right)\right] \\ -\frac{1}{l}\left[2 - 6\left(\frac{x}{l}\right)\right] \end{bmatrix} \tag{13}$$

which is simply the shape function matrix for a beam augmented by a zero term. Thus, the element stiffness matrix will be

$$[K^e] = \frac{EI}{l^3}\begin{bmatrix} 0 & 0 & 0 & 0 & 0 \\ 0 & 12 & 6l & -12 & 6l \\ 0 & 6l & 4l^2 & -6l & 2l^2 \\ 0 & -12 & -6l & 12 & -6l \\ 0 & 6l & 2l^2 & -6l & 4l^2 \end{bmatrix} \tag{14}$$

For the purpose of illustration, the assembled mass and stiffness matrices of the system for two elements after reduction would look like

$$[M] = \begin{bmatrix} I_h + M^1_{\theta\theta} + M^2_{\theta\theta} & M^1_{\theta w}(1,3) + M^2_{\theta w}(1,1) & M^1_{\theta w}(1,4) + M^2_{\theta w}(1,2) & M^2_{\theta w}(1,3) + M_{\theta t}(1,3) & M^2_{\theta w}(1,4) + M_{\theta t}(1,4) \\ & M^1_{ww}(3,3) + M^2_{ww}(1,1) & M^1_{ww}(3,4) + M^2_{ww}(1,2) & M^2_{ww}(1,3) & M^2_{ww}(1,4) \\ & & M^1_{ww}(4,4) + M^2_{ww}(2,2) & M^2_{ww}(2,3) & M^2_{ww}(2,4) \\ & & & M^2_{ww}(3,3) + M_{wt}(3,3) & M^2_{ww}(3,4) \\ \text{symmetric} & & & & M^2_{ww}(4,4) + M_{wt}(4,4) \end{bmatrix} \tag{15}$$

$$[K] = \begin{bmatrix} 0 & 0 & 0 & 0 & 0 \\ & K^1_{ww}(3,3) + K^2_{ww}(1,1) & K^1_{ww}(3,4) + K^2_{ww}(1,2) & K^2_{ww}(1,3) & K^2_{ww}(1,4) \\ & & K^1_{ww}(4,4) + K^2_{ww}(2,2) & K^2_{ww}(2,3) & K^2_{ww}(2,4) \\ & & & K^2_{ww}(3,3) & K^2_{ww}(3,4) \\ & \text{symmetric} & & & K^2_{ww}(4,4) \end{bmatrix} \tag{16}$$

The assembled and reduced system variables are now

$$\mathbf{q} = \begin{bmatrix} \theta \\ w_2 \\ \theta_2 \\ w_3 \\ \theta_3 \end{bmatrix} \tag{17}$$

where w_n and θ_n are the deflection and rotation variables of the nodes.

A. Piezoelectric Elements in Full System Model

The piezoelectric elements are bonded to both the bottom and top of the beam, and are assumed to have two structural degrees of freedom like the regular beam element. In addition, the piezoelectric element has one electrical degree of freedom which is the voltage. This single degree of freedom is due to the fact that the voltage generated by the piezoelectric is constant over the electrode. The single electrical degree of freedom is used as a sensor or actuator voltage when the material is used as a sensor or actuator.

Voltage can be used as a control input to the actuator, which will cause the actuator to apply moments that are equal and opposite to each other at either end of the element. The bending moment resulting from the voltage input will add a positive bending moment at node 2 and a negative bending moment at node 1. It is assumed that the displacement functions of the PZT will remain the same as that of the regular beam element and that the moments exerted by the piezoelectric actuator act at the nodal points.

In derivation of the piezoelectric beam element, it is assumed that the sensor and actuator have the same width and thickness, and form a collocated sensor-actuator pair. With this assumption, the piezoelectric beam element can be seen as a sandwich with the regular beam element in the middle with a piezoelectric element bonded on top of it (as actuator) and a piezoelectric element bonded underneath it (as sensor). More details of this method can be found in [9,36].

Making the same assumptions as for the derivation of the regular beam element, the piezoelectric beam element mass matrix can be obtained as

$$[M^{pe}] = \rho A \int_0^l [N]^T [N]\,\mathrm{d}x \tag{18}$$

where

$$\rho A = \rho_b b_b t_b + 2\rho_p b_p t_p \tag{19}$$

where l is the length of the piezoelectric element, b_b is the height (or width of the beam), b_p is the width of the piezoelectric material, ρ_b is the density of the beam, ρ_p is the density of the piezoelectric material, t_b is the thickness of the beam, and t_p is the thickness of the piezoelectric patch. Upon inspection, it can be clearly seen that the mass matrix of the piezoelectric element can be written as

$$[M^{pe}] = [M^e] + 2[M^e_p] \tag{20}$$

which is the sum of the mass matrix of the regular element, $[M^e]$, plus the mass matrix for the piezoelectric elements on the top and bottom of the beam, $[M^e_p]$.

The piezoelectric beam element stiffness matrix can be obtained as

$$[K^{pe}] = EI \int_0^l [B]^T [B]\,\mathrm{d}x \tag{21}$$

where $EI = E_b I_b + 2E_p I_p$, E_b is Young's modulus for the beam, I_b is the inertia of the beam, E_p is Young's modulus for the piezoelectric material, and I_p is the inertia of the piezoelectric element with respect

to the neutral axis of the beam. From the parallel axis theorem, $I_p = \frac{1}{12} b_p t_p^3 + b_p t_p((t_p + t_b)/2)^2$.

As for the mass matrix, $[K^{pe}]$ can also be written as

$$[K^{pe}] = [K^e] + 2[K_p^e] \tag{22}$$

provided that the inertia of the piezoelectric component is properly defined.

1. Piezoelectric Sensor Equations

The equations for a piezoelectric sensor can be derived from the direct piezoelectric equation under the assumption that there is no external electric field applied to the sensor layer. Thus, the electric displacement is directly proportional to the strain acting on it. For the sensor, the poling will be done along the thickness direction with electrodes on the upper and lower surfaces. Thus, the only nonzero electric displacement component is D_z, which is given by (assuming no external electric field)

$$D_z = d_{31}\sigma_1 \tag{23}$$

From Hooke's law in one dimension, it is known that the stress is related to the strain through the modulus of elasticity, E, as

$$\sigma_1 = E\epsilon_1 \tag{24}$$

Therefore, the electric displacement becomes

$$D_z = d_{31}E_p\epsilon_1 \tag{25}$$

where d_{31} is the relevant electric displacement coefficient. The total charge developed by the strain in the structure will be

$$q = \iint_A D_z \, \mathrm{d}A \tag{26}$$

which upon substitution for D_z becomes

$$q = d_{31}E_p b_p \int_0^l \epsilon_1 \, \mathrm{d}x \tag{27}$$

Since the strain in Euler–Bernoulli beam theory has only one nonzero component of strain, which is along the x-axis, the strain through the beam is given by (here, for simplicity in the derivation, the coordinate corresponding to the rigid mode has been omitted from $\mathbf{q}$ and only the flexible structure is considered)

$$\epsilon_1 = \epsilon = \left(\frac{t_b}{2} + t_p\right)[B]\mathbf{q} \tag{28}$$

which upon substitution into the equation for charge [36] becomes

$$q = d_{31}E_p b_p \left(\frac{t_b}{2} + t_p\right) \int_0^l [B]\mathbf{q} \, \mathrm{d}x \tag{29}$$

and evaluating gives

$$q = d_{31}E_p b_p \left(\frac{t_b}{2} + t_p\right)[0 \quad -1 \quad 0 \quad 1]\mathbf{q} \tag{30}$$

The capacitance of the piezoelectric sensor [37] can be shown as

$$C = \frac{l b_p e_{33}^{\sigma}}{t_p} \tag{31}$$

which means that the voltage generated by the sensor is given as

$$V_s = G_s \frac{Q}{C_p} = \frac{G_s d_{31} E_p t_p (\frac{t_b}{2} + t_p)[0 \quad -1 \quad 0 \quad 1]\mathbf{q}}{l e_{33}^{\sigma}} \tag{32}$$

where G_s is the sensor signal conditioning gain. Letting

$$\mathbf{p} = \frac{G_s d_{31} E_p t_p (\frac{t_b}{2} + t_p)}{l e_{33}^{\sigma}} \begin{bmatrix} 0 \\ -1 \\ 0 \\ 1 \end{bmatrix} \tag{33}$$

the equation for the voltage developed can be simplified to

$$V_s(t) = \mathbf{p}^T\mathbf{q} \tag{34}$$

2. Piezoelectric Actuator Equations

For the piezoelectric actuator, the sensor voltage is typically applied as a control signal to the actuator after being modified by a control law, and then multiplied by another gain G_a, which is usually supplied by means of an amplifier. Therefore the actuator voltage is given by

$$V_a(t) = G_a V_{\text{in}}(t) \tag{35}$$

The applied electric field in the actuator is due to the applied voltage, therefore the electric field is given by

$$E_f = \frac{V_a(t)}{t_p} \tag{36}$$

The strain created in the actuator by the applied electric field can then be described as

$$\epsilon_a = d_{31}E_f \tag{37}$$

and once again using Hooke's law in one dimension gives the stress as

$$\sigma_a = \frac{E_p d_{31} V_a(t)}{t_p} \tag{38}$$

Because of the stress in the structure, bending moments will act in an equal and opposite manner at the two nodal points. Since the piezoelectric element will typically have a small cross section, it is assumed that the moments exerted by the patch essentially act at the nodal points [36]. The expression for the bending moment in the small cross section is given by

$$M_a = \int_{\frac{t_b}{2}}^{\frac{t_b}{2}+t_p} \sigma_a z \, \mathrm{d}z \tag{39}$$

which upon substitution for the stress gives

$$M_a = \frac{E_p d_{31} V_a(t)}{t_p} \int_{\frac{t_b}{2}}^{\frac{t_b}{2}+t_p} z \, \mathrm{d}z \tag{40}$$

which upon evaluation of the integral gives

$$M_a = E_p d_{31} V_a(t) \left(\frac{t_p + t_b}{2}\right) \tag{41}$$

The control force, or force exerted by the actuators due to the applied control voltage can be derived as (here again note that the rigid coordinate has been omitted)

$$\mathbf{f}_p = E_p d_{31} b_p V_a(t) \left(\frac{t_p + t_b}{2}\right) \int_0^l [N']^T \, \mathrm{d}x \tag{42}$$

which after carrying through the integration and substituting in Eq. (35) becomes

$$\mathbf{f}_p = E_p d_{31} b_p G_a V_{\text{in}}(t) \left(\frac{t_p + t_b}{2}\right) \begin{bmatrix} -1 \\ 0 \\ 1 \\ 0 \end{bmatrix} \tag{43}$$

Letting

$$\mathbf{h} = G_a E_p d_{31} b_p \left(\frac{t_p + t_b}{2}\right) \begin{bmatrix} -1 \\ 0 \\ 1 \\ 0 \end{bmatrix} \tag{44}$$

the control force equation becomes

$$\mathbf{f}_p = \mathbf{h} V_{\text{in}}(t) \tag{45}$$

B. Additional Piezoelectric Considerations

For completeness it should be noted that the vectors **p** and **h** will have all of their elements shifted down one position to make room for a zero at the location of the first element corresponding to the fact that their influence is not exerted at the location of the hub.

C. System Assembly, Reduction, and Modal Decoupling

The entire second-order differential equation can be assembled using the standard finite element technique with Rayleigh damping included as

$$[M]\ddot{\mathbf{q}} + [D]\dot{\mathbf{q}} + [K]\mathbf{q} = \mathbf{F} \tag{46}$$

where $[M]$, $[D]$, and $[K]$ are the global mass, damping, and stiffness matrices.

Modal decoupling can be performed to obtain the normal mode system through similarity transformations [38] giving

$$\ddot{\mathbf{x}} + Z\dot{\mathbf{x}} + \Omega\mathbf{x} = S_m^T \mathbf{F} \tag{47}$$

III. Control System Design

The slewing motion of the hub is controlled using a simple proportional-derivative (PD) feedback law as

$$\tau(t) = K_p(\theta_d - \theta) + K_d(\dot{\theta}_d - \dot{\theta}) \tag{48}$$

where θ is the actual hub angle, θ_d is the desired angle, K_p and K_d are the proportional and derivative gains, respectively.

Of course for either disturbance rejection or step-following, the slewing motion of the hub generates vibrations in the flexible appendage which need to be controlled using other control laws. To do this, the PD controller will be combined with input shaping.

A. Input Shaping

Basically, any type of input shaper can be combined with the proposed multimode adaptive PPF control for vibration suppression. Here, for simplicity, three simple shapers (ZV, ZVD, and ZVDD) will be used in the following simulations.

The ZV shaper is a two-impulse input shaper that can achieve zero-vibration after the last (second) impulse. The amplitudes and time instants of two impulses are as follows:

$$A_1 = \frac{1}{1+K}, \qquad t_1 = 0 \qquad A_2 = \frac{K}{1+K}, \qquad t_2 = \frac{\pi}{\omega_d}$$

where $K = \exp(-((\xi\pi)/\sqrt{1-\xi^2}))$, ξ is the damping ratio, ω_d is the damped natural frequency.

ZV shaper can be used to achieve zero-vibration if the natural frequency and damping ratio are known exactly. However, the residual vibration will be big if the uncertainty in the natural frequency is big. In other words, the ZV shaper is not robust.

The robustness of the input shaper to uncertainty in system's natural frequencies can be increased by setting the derivative to zero. Setting the derivative to zero is the equivalent of producing small changes in vibration with corresponding changes in the natural frequency [39]. This yields a three-impulse ZVD shaper with parameters

$$A_1 = \frac{1}{1+2K+K^2}, \qquad t_1 = 0$$
$$A_2 = \frac{2K}{1+2K+K^2}, \qquad t_2 = \frac{\pi}{\omega_d}$$
$$A_3 = \frac{K^2}{1+2K+K^2}, \qquad t_3 = 2t_2$$

The robustness of the input shaper can further be increased by setting the second derivative to zero. Similarly, this yields a four-impulse ZVDD shaper with parameters

$$A_1 = \frac{1}{1+3K+3K^2+K^3}, \qquad t_1 = 0$$
$$A_2 = \frac{3K}{1+3K+3K^2+K^3}, \qquad t_2 = \frac{\pi}{\omega_d}$$
$$A_3 = \frac{3K^2}{1+3K+3K^2+K^3}, \qquad t_3 = 2t_2$$
$$A_4 = \frac{K^3}{1+3K+3K^2+K^3}, \qquad t_4 = 3t_2$$

The sensitivity curves for these three input shapers are shown in Fig. 3. It can be seen that, for the same residual vibration level, the ZVDD shaper allows much more uncertainty in the frequency than the ZV shaper.

B. Positive Position Feedback

Considering the scalar case first, PPF can be described by two coupled differential equations where the first equation describes the structure, and the second describes the compensator [8] as

$$\ddot{\xi} + 2\zeta\omega\dot{\xi} + \omega^2\xi = g\omega^2\eta \qquad \ddot{\eta} + 2\zeta_f\omega_f\dot{\eta} + \omega_f^2\eta = \omega_f^2\xi \tag{49}$$

where ξ is the modal coordinate, η is the filter coordinate, ζ and ζ_f are the structural damping and filter damping ratios, ω and ω_f are the structural natural frequency and filter frequency, and g is the scalar gain. It is shown in [8] that the necessary and sufficient condition for stability is

$$0 < g < 1 \tag{50}$$

The next major advantage of the PPF is that the transfer function of the controller rolls off quickly, as can be seen from its Bode plot in Fig. 4. This is good because it makes the PPF controller well suited for control of low-frequency modes of a structure with well-separated modes. This is also a major advantage due to the fact that the system will not be influenced by unmodeled high frequency dynamics.

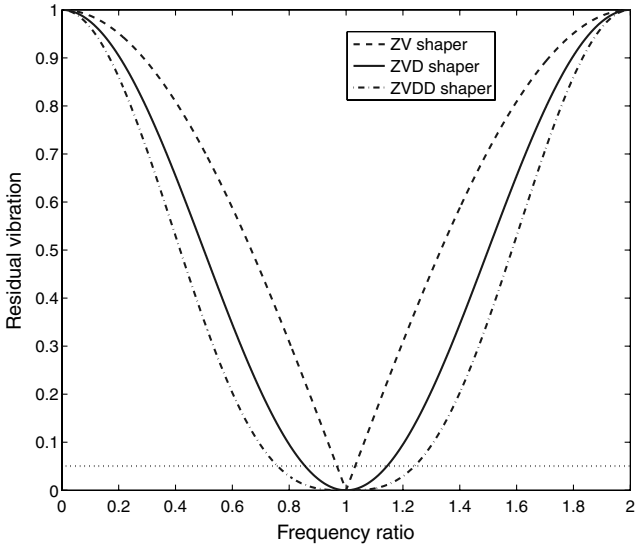

Fig. 3 Sensitivity curves of various input shapers.

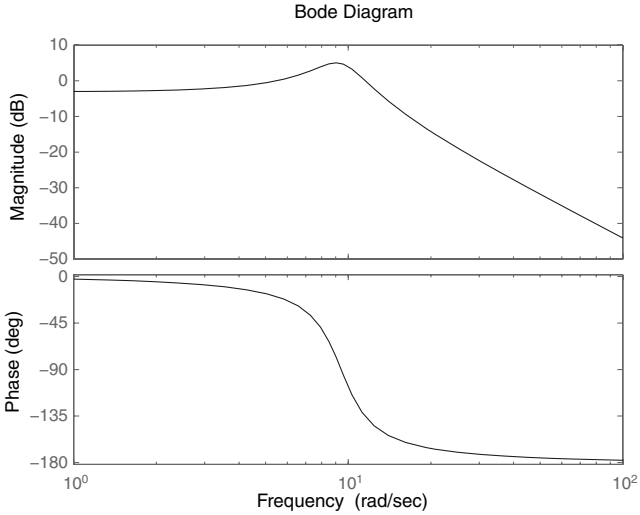

Fig. 4 Bode plot for a single mode PPF controller.

There are three possible output conditions for a PPF controller based upon the choice of controller frequency ω_c [10]: active flexibility, active damping, or active stiffness. To effectively damp out a structural mode, obviously the case of active damping is required. Thus the controller frequency should be selected to be close to the modal frequency.

In theory, a flexible manipulator has infinite vibrational modes, and sometimes there is more than one dominant mode. To damp the dominant modes, multiple PPF controllers are required in parallel, where each controller is tuned to the natural frequency of the mode it is to damp. In our system, the first two vibration modes are dominant and need to be suppressed. This means that the frequency of η_1 is chosen to be close to that of ξ_1 while the frequency of η_2 is chosen to be close to that of ξ_2.

For the general multivariable case, the system of equations becomes

$$\ddot{\boldsymbol{\xi}} + D\dot{\boldsymbol{\xi}} + \Omega\boldsymbol{\xi} = C^T G\boldsymbol{\eta} \qquad \ddot{\boldsymbol{\eta}} + D_f\dot{\boldsymbol{\eta}} + \Omega_f\boldsymbol{\eta} = \Omega_f C\boldsymbol{\xi} \tag{51}$$

where G is the diagonal gain matrix, C is the participation matrix, Ω and Ω_f are the diagonal modal and filter frequency matrices, and D and D_f are the diagonal modal and filter damping matrices. In this case, stability can be guaranteed [8] if and only if

$$\Omega - C^T GC > 0 \tag{52}$$

where greater than zero means positive definite. Another important property of PPF is that all spillover into uncontrolled or unmodeled modes is stabilizing [8].

Considering for a moment, only the flexible modes of the structure, a PPF controller is developed in this section for the beam using a single collocated PZT sensor/actuator pair. The dynamic equation of the structure in modal coordinates is

$$\ddot{x} + Z_s\dot{x} + \Omega_s x = S_m^T h u \tag{53}$$

where x is the vector of modal coordinates, Z_s is the damping matrix, Ω_s is the frequency matrix, S_m^T is the matrix of mass normalized eigenvectors of the system, h is the actuator influence matrix, and u is the input to the actuator (voltage in this case). The sensor (or output) equation can be seen as

$$y = p^T S_m x \tag{54}$$

where p is the sensor influence matrix.

The equation describing the controller is given as

$$\ddot{\eta} + Z_f\dot{\eta} + \Omega_f\eta = \Omega_f E y \tag{55}$$

where η is the vector of controller coordinates, Z_f is the controller damping matrix, Ω_f is the controller frequency matrix, and E is the modal participation factor matrix, which will be defined shortly. The actuator input equation is given as

$$u = E^T G\eta \tag{56}$$

where G is the gain matrix.

Since S_m^T is the matrix of mass normalized eigenvectors, the modal participation factor matrix can be defined as

$$E = S_m^T M r \tag{57}$$

where M is the global mass matrix of the system, and r is a matrix of ones with the same number of rows as M, and the number of columns equal to the number of collocated sensor/actuator pairs.

The four equations, i.e. Eqs. (53–56), describing the system can be combined into two second-order differential equations as

$$\ddot{x} + Z_s\dot{x} + \Omega_s x = S_m^T h E^T G\eta \tag{58}$$

$$\ddot{\eta} + Z_f\dot{\eta} + \Omega_f\eta = \Omega_f E p^T S_m x \tag{59}$$

Now the structure and controller equations will be placed into state space (or first-order form) for ease of analysis. The structural equations become

$$\dot{\hat{x}} = A\hat{x} + Bu \tag{60}$$

$$y = C\hat{x} \tag{61}$$

where

$$A = \begin{bmatrix} 0 & I \\ -\Omega_s & -Z_s \end{bmatrix} \qquad B = \begin{bmatrix} 0 \\ S_m^T h \end{bmatrix} \qquad C = [\, p^T S_m \quad 0\,]$$

and the controller equations become

$$\dot{\hat{\eta}} = \hat{A}\,\hat{\eta} + \hat{B}y \tag{62}$$

$$u = \hat{C}\,\hat{\eta} \tag{63}$$

where

Table 1 System and simulation parameters

Parameter	Value	Description
I_h	10 kg · m^2	Hub inertia
b	0.11715 m	Hub radius
l	1.1365 m	Length of the beam
t	0.00258 m	Thickness of the beam
h	0.0828 m	Height of the beam
ν	0.33	Poisson's ratio of the beam
ρ	2700 kg/m^3	Density of the beam
E	70 GPa	Modulus of elasticity for the beam
l_p	0.05084 m	Length of the piezoelectric
b_p	0.03806 m	Width of the piezoelectric
t_p	0.00038 m	Thickness of the piezoelectric
ν_p	0.3	Poisson's ratio of the piezoelectric
ρ_p	7700 kg/m^3	Density of the piezoelectric
E_p	68 GPa	Modulus of elasticity for the piezoelectric
nElements	20	Number of elements used
m_{tip}	0	Tip mass
I_{tip}	0	Inertia of tip mass
K_p	55	Proportional gain
K_d	45	Derivative gain
$\hat{\Phi}_0$	$[1 \;\; 1 \;\; 1 \;\; 1 \;\; 1 \;\; 1 \;\; 1]^T$	Initial parameter guess

$$\hat{A} = \begin{bmatrix} 0 & I \\ -\Omega_f & -Z_f \end{bmatrix} \qquad \hat{B} = \begin{bmatrix} 0 \\ \Omega_f E \end{bmatrix} \qquad \hat{C} = [E^T G \quad 0]$$

C. Adaptive Parameter Estimation

Since the structural transfer function is single-input and single-output, it can be put in transfer function form through

$$G(s) = \frac{Z(s)}{R(s)} = C(sI - A)B \tag{64}$$

where

$$R(s) = s^n + a_{n-1}s^{n-1} + \cdots + a_1 s + a_0 \tag{65}$$

$$Z(s) = b_m s^m + \cdots + b_1 s + b_0 \tag{66}$$

which allows the adaptive law to be developed generically.

The output of the system is of the following form:

$$y = G(s)u = \frac{Z(s)}{R(s)}u \tag{67}$$

where u is the input of the plant, and the output can also be expressed as [40]

$$y^{(n)} + a_{n-1}y^{(n-1)} + \cdots + a_1\dot{y} + a_0 y = b_m u^{(m)} + \cdots + b_1\dot{u} + b_0 u \tag{68}$$

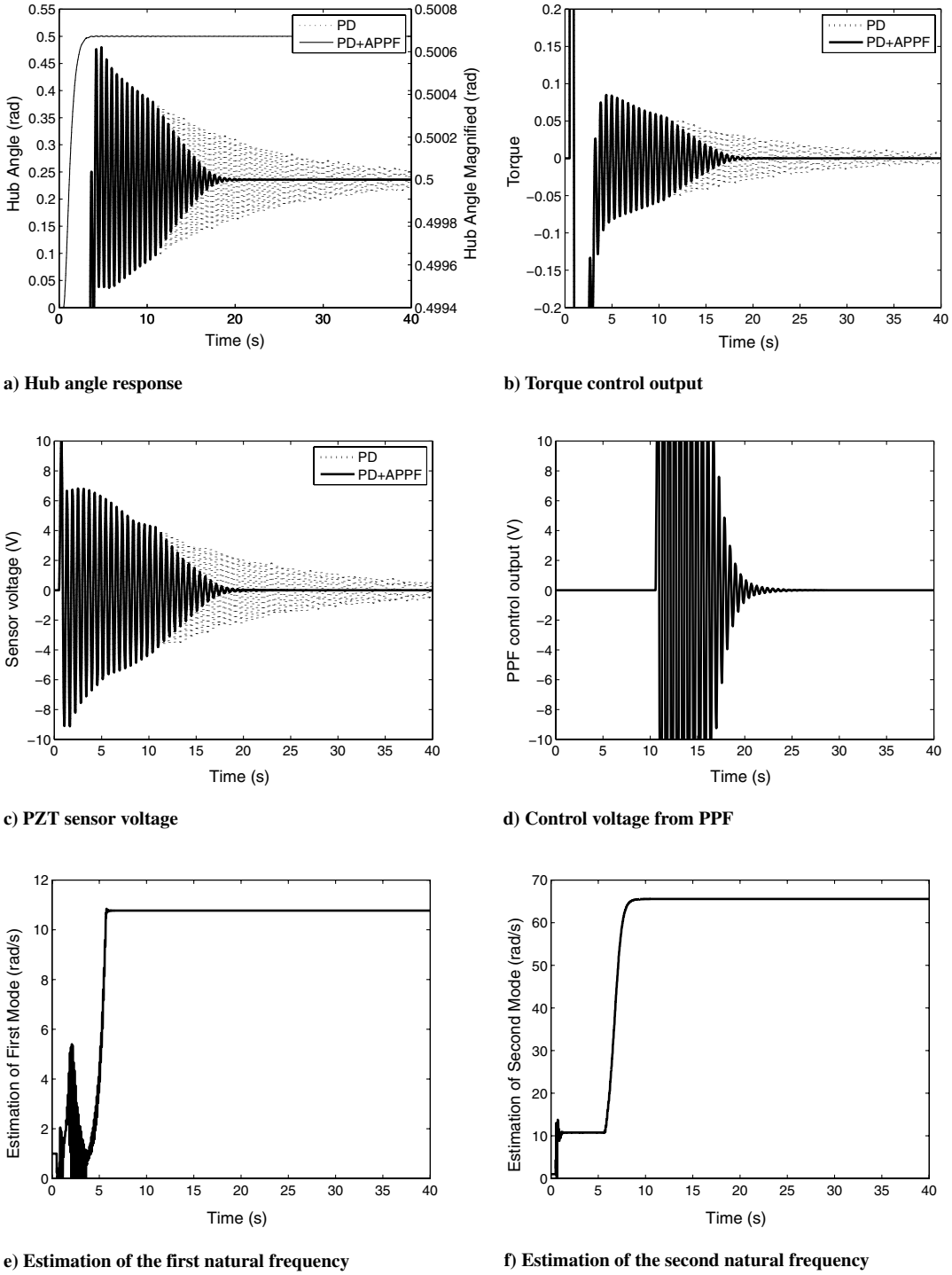

a) Hub angle response

b) Torque control output

c) PZT sensor voltage

d) Control voltage from PPF

e) Estimation of the first natural frequency

f) Estimation of the second natural frequency

Fig. 5 Simulation results of PD control with multimode adaptive PPF.

Lumping all of the unknown parameters into the vector

$$\Phi = [\, b_m \quad \cdots \quad b_0 \quad a_{n-1} \quad \cdots \quad a_0 \,]^T \tag{69}$$

and filtering both sides of Eq. (68) with the following monic Hurwitz polynomial [40]

$$\frac{1}{\Lambda(s)} = \frac{1}{s^n + \lambda_{n-1}s^{n-1} + \cdots + \lambda_1 s + \lambda_0} \tag{70}$$

the static parametric model can be obtained as [40]

$$z = \Phi^T \phi \tag{71}$$

where

$$z = \frac{s^n}{\Lambda(s)} y$$

$$\phi = \left[\frac{s^m}{\Lambda(s)} u \quad \cdots \quad \frac{1}{\Lambda(s)} u \quad -\frac{s^{n-1}}{\Lambda(s)} y \quad \cdots \quad -\frac{1}{\Lambda(s)} y \right]^T$$

The estimation model can now be defined as

$$\hat{z} = \hat{\Phi}^T \phi \tag{72}$$

where $\hat{z}$ and $\hat{\Phi}$ is the estimate of z and Φ at each time t. The estimation error can then be defined as

$$\epsilon = \frac{z - \hat{z}}{m_s^2} = \frac{z - \hat{\Phi}^T \phi}{m_s^2} \tag{73}$$

where m_s^2 is referred to as the normalizing signal and is designed to bound ϕ from above [40]. A typical choice for the normalizing signal is

$$m_s^2 = 1 + \alpha \phi^T \phi \tag{74}$$

where $\alpha > 0$.

The cost function is a convex function of $\hat{\Phi}$ with a global minimum and is given by

$$J(\hat{\Phi}) = \frac{1}{2}\int_0^t e^{-\beta(t-\tau)} \frac{[z(\tau) - \hat{\Phi}^T(t)\phi(\tau)]^2}{m_s^2(\tau)}\, \mathrm{d}\tau + \frac{1}{2} e^{-\beta t} (\hat{\Phi} - \hat{\Phi}_0)^T Q_0 (\hat{\Phi} - \hat{\Phi}_0) \tag{75}$$

where $Q_0 = Q_0^T > 0$, $\beta > 0$ are design constants, and $\hat{\Phi}_0 = \hat{\Phi}(0)$ is the initial parameter estimates of the unknowns.

This cost function serves to deweight previous data and includes a penalty on the error in the initial guess. Following the derivation presented by Ioannou and Fidan [40], the recursive least-squares algorithm with forgetting factor is obtained as

$$\dot{\hat{\Phi}} = P \epsilon \phi \tag{76}$$

$$\dot{P} = \begin{cases} \beta P - P \frac{\phi \phi^T}{m_s^2} P & \|P\| \le R_0 \\ 0 & \text{otherwise} \end{cases} \tag{77}$$

where $P(0) = P_0 = Q_0^{-1}$. Here, R_0 is a scalar that serves as an upper bound for $\|P\|$, since in this case, with $\beta > 0$, $P(t)$ may grow without bound.

D. Combining the System

Considering the full system, the state space model can be transformed into transfer function form through the relation

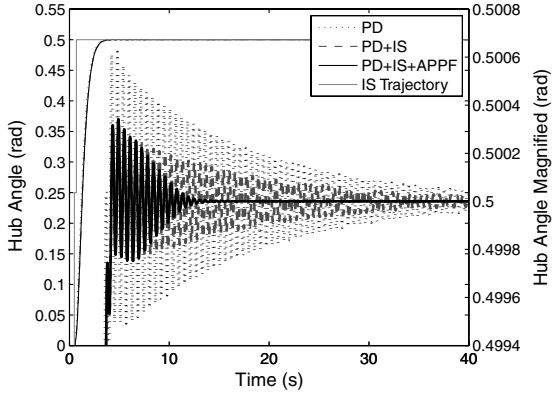

a) Hub angle response

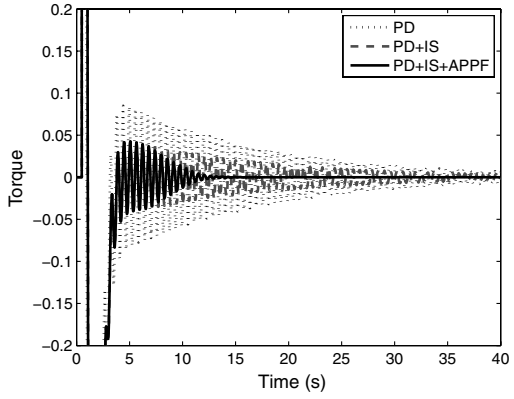

b) Torque control output

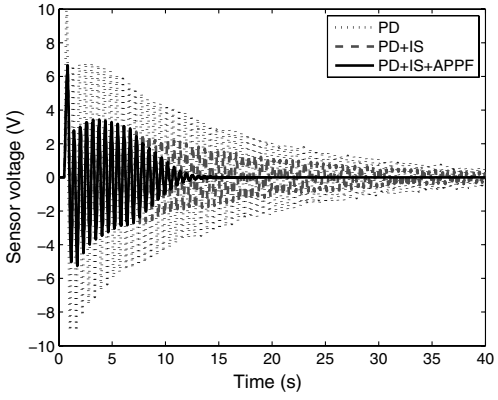

c) PZT sensor voltage

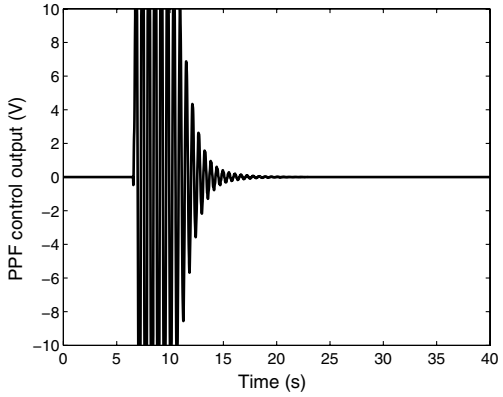

d) Control voltage from PPF

Fig. 6 Simulation results with multimode adaptive PPF and ZV input shaper (frequency uncertainty: +50%).

$$H(s) = C(sI - A)^{-1}B + D \tag{78}$$

Because of the fact that there are two outputs (hub angle and sensor voltage) and two inputs (torque and actuator voltage) in the system, $H(s)$ becomes a 2×2 transfer function matrix, given for the open loop by

$$\begin{bmatrix} \theta(s) \\ V_s(s) \end{bmatrix} = \begin{bmatrix} G_{11}(s) & G_{12}(s) \\ G_{21}(s) & G_{22}(s) \end{bmatrix} \begin{bmatrix} \tau \\ V_c \end{bmatrix} \tag{79}$$

As a generic case, which can be extended or simplified with relative ease, the system is chosen to consider the rigid mode and two flexible modes with A, B, and C given as

$$A = \begin{bmatrix} 0 & 0 & 0 & 1 & 0 & 0 \\ 0 & 0 & 0 & 0 & 1 & 0 \\ 0 & 0 & 0 & 0 & 0 & 1 \\ 0 & 0 & 0 & 0 & 0 & 0 \\ 0 & -\Omega_1 & 0 & 0 & -z_1 & 0 \\ 0 & 0 & -\Omega_2 & 0 & 0 & -z_2 \end{bmatrix}, \quad B = \begin{bmatrix} 0 & 0 \\ 0 & 0 \\ 0 & 0 \\ a & b \\ c & d \\ e & f \end{bmatrix}$$

$$C = \begin{bmatrix} p & q & r & 0 & 0 & 0 \\ t & u & v & 0 & 0 & 0 \end{bmatrix}$$

In this case, the four transfer functions can be found through Eq. (78) as

$$G_{11}(s) = \frac{m_1 s^4 + m_2 s^3 + m_3 s^2 + m_4 s + m_5}{s^2(s^2 + z_1 s + \Omega_1)(s^2 + z_2 s + \Omega_2)}$$

$$G_{12}(s) = \frac{(qd + rf)s^2 + (rfz_1 + qdz_2)s + (rf\Omega_1 + qd\Omega_2)}{(s^2 + z_1 s + \Omega_1)(s^2 + z_2 s + \Omega_2)}$$

$$G_{21}(s) = \frac{(uc + ve)s^2 + (vez_1 + ucz_2)s + (ve\Omega_1 + uc\Omega_2)}{(s^2 + z_1 s + \Omega_1)(s^2 + z_2 s + \Omega_2)}$$

$$G_{22}(s) = \frac{(ud + vf)s^2 + (vfz_1 + udz_2)s + (vf\Omega_1 + ud\Omega_2)}{(s^2 + z_1 s + \Omega_1)(s^2 + z_2 s + \Omega_2)}$$

where $m_1 = (qc + re + pa)$, $m_2 = (rez_1 + qcz_2 + paz_1 + paz_2)$, $m_3 = (pa\Omega_2 + paz_1z_2 + re\Omega_1 + pa\Omega_1 + qc\Omega_2)$, $m_4 = (paz_1\Omega_2 + pa\Omega_1z_2)$, and $m_5 = pa\Omega_1\Omega_2$. In the simplification of the last three transfer functions the fact that b and t tend to zero have been used to reduce the order of the individual transfer functions. This simplification is made due to the fact that if b tends to zero, this implies that control voltage on the piezos does not directly affect the hub angle, and with t tending to zero implies that the hub angle does not directly affect the sensor voltage produced.

For the control system, the step command is shaped by an input shaper outside of the loop, with a PD controller inside the closed loop for the rigid hub motion. The estimator is on at the beginning with arbitrary initial guesses, and is set up to adapt on $G_{21}(s)$, which is between the sensor voltage and the torque. The estimator is modified to turn off when the error

$$\epsilon = \frac{z - \hat{z}}{m_s^2} = \frac{z - \hat{\Phi}^T \phi}{m_s^2} < 0.1 \tag{80}$$

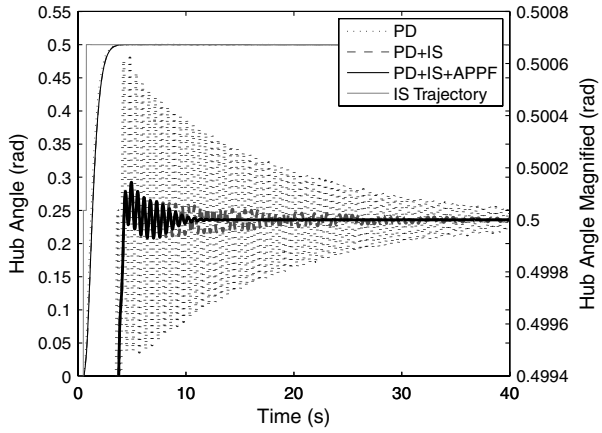

a) Hub angle response

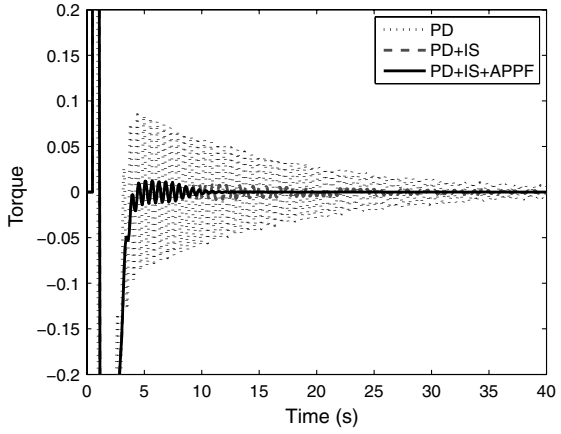

b) Torque control output

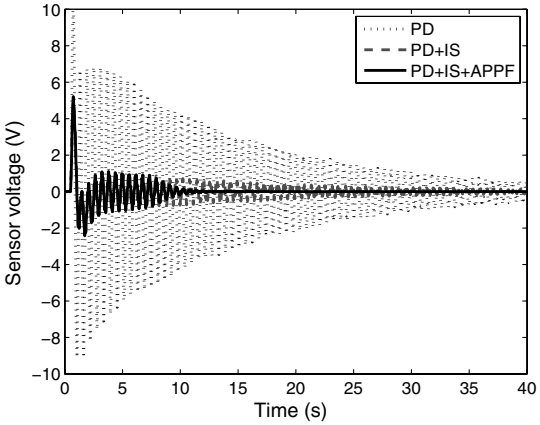

c) PZT sensor voltage

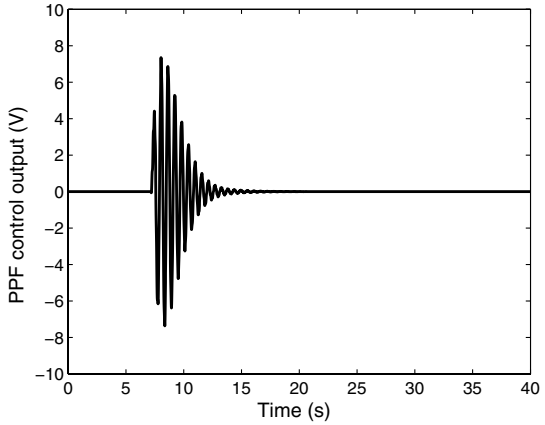

d) Control voltage from PPF

Fig. 7 Simulation results with multimode adaptive PPF and ZV input shaper (frequency uncertainty: +10%).

for longer than 1 s, and then to turn on the multimode adaptive PPF controller. This is done since at this point, the parameter estimates will have converged within a reasonable amount (as ϵ represents the difference between the actual transfer function and estimated transfer function), and adaptation is no longer needed. The second reason this is done, is that after a few seconds of running, the PPF controller may start to eliminate the vibrations in the structure and the persistence of excitation condition may no longer be valid, leading to possibly erroneous estimates of the natural frequencies as control is applied.

IV. Simulation Results

The physical properties of the system and the simulation parameters are listed in Table 1. Finite element analysis shows that the actual frequencies of the first two vibration modes are 1.7141 and 10.4337 Hz, and they are assumed to be known with uncertainties. It is desired to slew the rigid hub 0.5 radians which is done by a PD control law. Saturation is included on the input and output of the PZT sensor and actuator at ± 10 V to keep the system physically realistic.

In this study, three simulation scenarios are considered: 1) PD control only; 2) PD control with adaptive PPF; and 3) PD control with input shaping and adaptive PPF.

First, PD feedback is applied to control the hub angle, however, neither input shaping nor multimode adaptive PPF is used. Since no active vibration control is used, the vibration of the flexible beam is big, as seen in Fig. 5.

To suppress flexible vibration, in the next simulation, the proposed multimode adaptive PPF controller is employed to suppress the vibration of the first two modes. PD feedback is used to control the hub angle motion. The simulation results are shown in Fig. 5 for comparison. It can be seen from the simulation results that the flexible vibration has been suppressed to a very low level after 18 s using the proposed adaptive PPF controller. Also, it shows that, at about 10 s, the parameter estimator successfully estimated the first two natural frequencies to be 1.7143 and 10.4327 Hz, respectively, which are very close to the true values. Once the estimation is done, the PPF controllers are turned on.

Finally, the input shaping and adaptive PPF are combined to suppress vibration. Input shaping is designed to suppress the first flexible vibration mode during slewing. Because of the frequency uncertainty, however, there will be residual vibration, which will be suppressed through the PZT actuator with multimode adaptive PPF. Here, three input shapers are used in the simulations, the ZV shaper, ZVD shaper, and ZVDD shaper. Moreover, two frequency uncertainty levels (10 and 50% high) are considered for the first vibration mode. For comparison purposes, PD control with input shaping is also applied to slew the manipulator in order to suppress the vibration. The simulation results have been included in the figures corresponding to which shaper the adaptive PPF is combined with.

Figures 6–11 show the hub angle response, torque control output, PZT sensor output, and PZT actuator control input for those simulations. Table 2 shows the estimated frequencies of the first two vibration modes and the times for the estimation to be done. It can be seen that 1) the frequencies of the first and second mode can be estimated accurately for all the cases; and 2) the vibrations have been suppressed very well and quickly by combining the input shaping and the adaptive PPF strategy.

In Fig. 6, the results of applying the ZV shaper, and the ZV shaper with the adaptive PPF can be seen for the case when the first mode is off by $+50\%$. The advantages of using the combined control law (PD + IS + APPF) can be seen as the ZV shaper alone will still have residual vibration at the end of the simulation, while the combined law has no residual vibration after roughly 12 s. When the frequency uncertainty is only $+10\%$ as in Fig. 7, the control with only the ZV

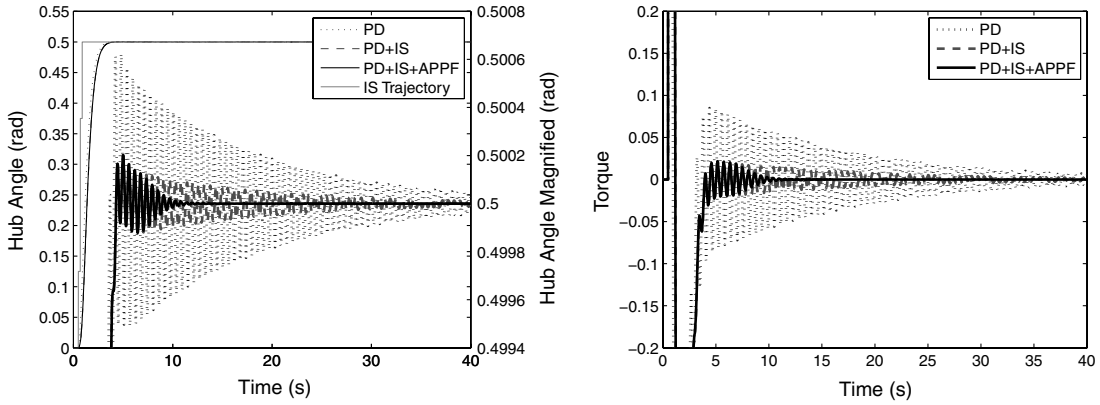

a) Hub angle response

b) Torque control output

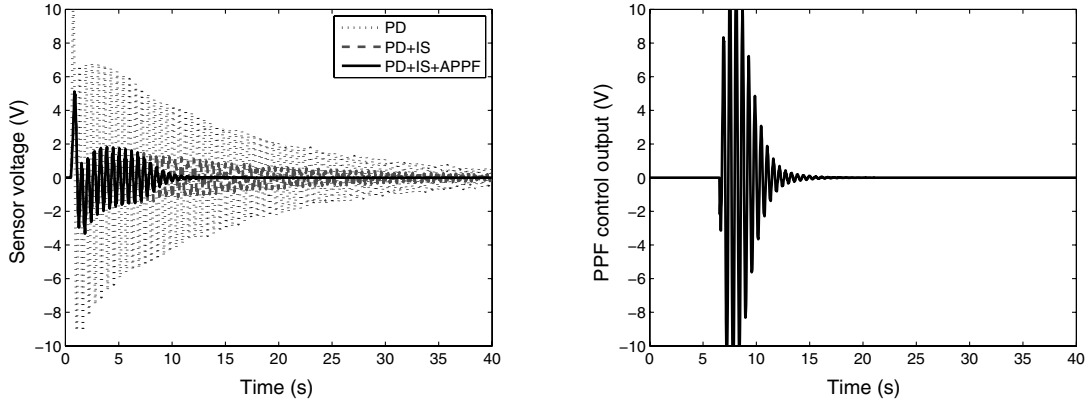

c) PZT sensor voltage

d) Control voltage from PPF

Fig. 8 Simulation results using multimode adaptive PPF and ZVD input shaper (frequency uncertainty: +50%).

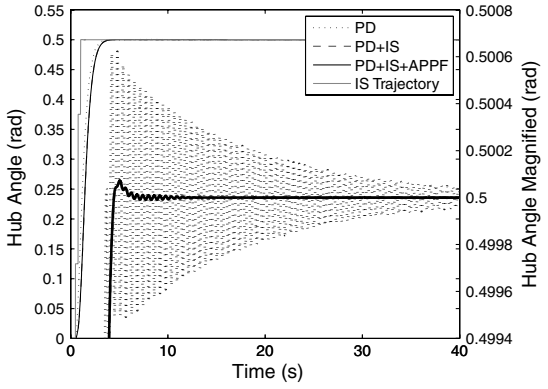

a) Hub angle response

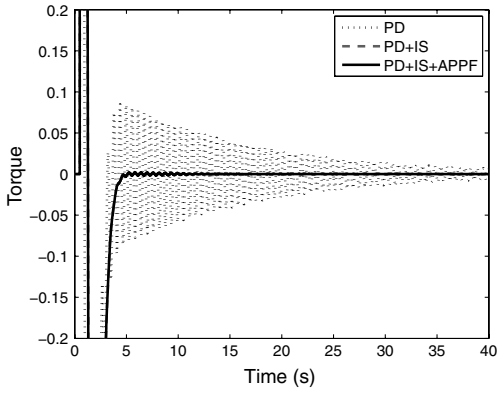

b) Torque control output

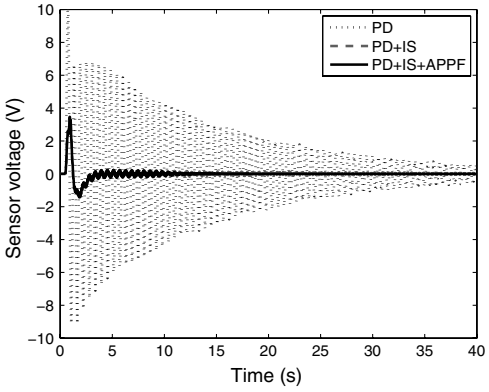

c) PZT sensor voltage

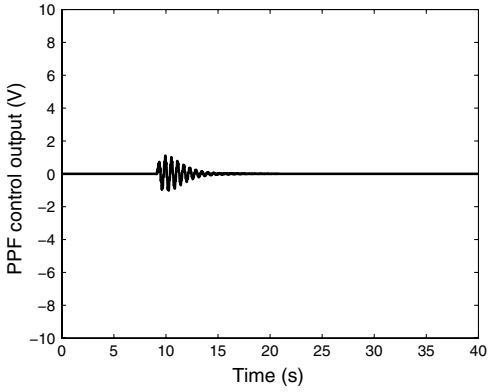

d) Control voltage from PPF

Fig. 9 Simulation results using multimode adaptive PPF and ZVD input shaper (frequency uncertainty: +10%).

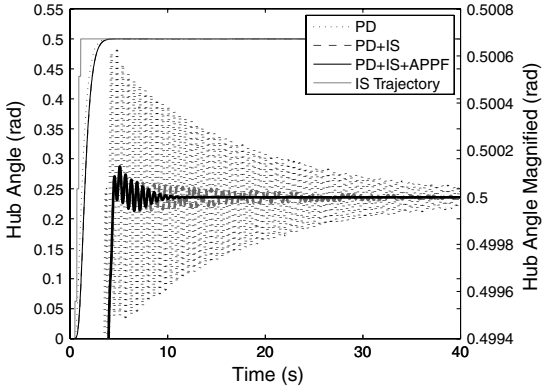

a) Hub angle response

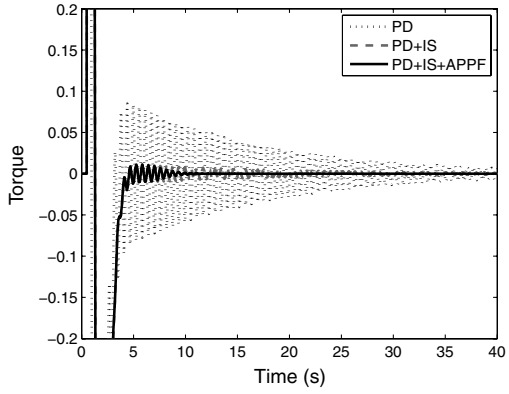

b) Torque control output

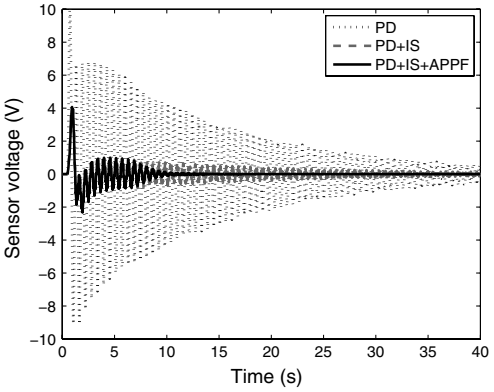

c) PZT sensor voltage

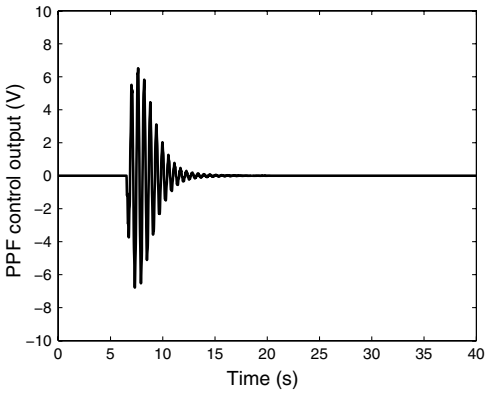

d) Control voltage from PPF

Fig. 10 Simulation results using multimode adaptive PPF and ZVDD input shaper (frequency uncertainty: +50%).

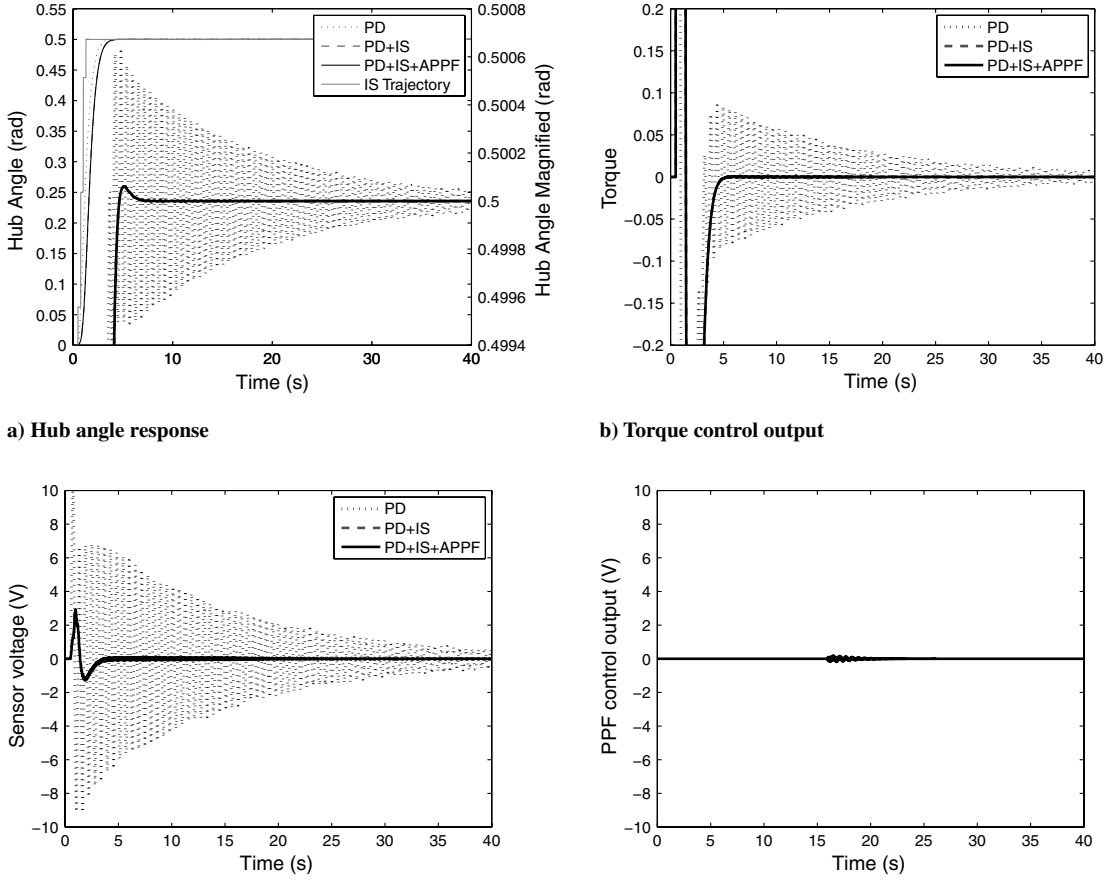

a) Hub angle response

b) Torque control output

c) PZT sensor voltage

d) Control voltage from PPF

Fig. 11 Simulation results with multimode adaptive PPF and ZVDD input shaper (frequency uncertainty: +10%).

shaper will again still have residual vibration at the end of the simulation (although at a much lower level than that of the previous case). Here, the combined law has damped out the residual vibrations of the manipulator in about 11 s.

In the next case, when the ZV shaper is replaced with a ZVD shaper, it is expected that the residual vibration will be lower for both cases. In Fig. 8 when the frequency error is +50%, it can again be seen that there will be residual vibration for the ZVD shaper control only at the end of the simulation, while again, with the combined law, it is damped out within 12 s. In Fig. 9 when the frequency error is +10%, the effect of the input shaper becomes much stronger, and there is only a small amount of residual vibration. Here again, however, in roughly 11 s, the combined law has suppressed the vibrations of the manipulator.

For the last shaper considered, the ZVDD, it is again expected that the amount of residual vibration will be smaller than that of the ZVD and ZV shaper due to the fact that it is more robust. For a frequency error of +50% in the shaper, it can be seen in Fig. 10 that with the ZVDD shaper, there is still residual vibration again at the end of the simulation, however, at a lower level than that of the ZVD shaper. When the ZVDD shaper is combined with the adaptive PPF law, the vibrations again have been removed in roughly 11 s. For the next case, when the error is +10% (in Fig. 11), the residual vibration is very, very small for the ZVDD shaper, and it could be argued that in experiment, this would be very difficult to pick up out of noise. The combined law again suppresses what little residual vibration there is left in the system.

The simulation results indicate that the proposed adaptation law works and can adapt to the actual parameter values. Moreover, the results show that better vibration suppression performance can be obtained by combining input shaping with the proposed multimode adaptive PPF controller. When the design frequency of an input shaper is close to the true value, the first vibration mode is more effectively suppressed and the second mode is not as excited by the slewing motion. As the initial value chosen for the first natural frequency of the system becomes less accurate, the vibration suppression capability of the input shaper obviously decreases and more vibrations are seen in the system, and here the multimode adaptive PPF algorithm shows its benefits. Also, as expected, as the robustness of an input shaper increases, the amount of system vibration decreases, even when the shapers are badly tuned.

V. Conclusions

In this paper, the dynamic modeling of a slewing flexible manipulator was performed using the finite element method through

Table 2 Estimation results of the first two frequencies, Hz

	Estimated frequencies	
Input shaper type	Frequency uncertainty: +50%	Frequency uncertainty: +10%
ZV	1.7141, 10.4323 (∼5 s)	1.7141, 10.4308 (∼6 s)
ZVD	1.7141, 10.4323 (∼6 s)	1.7141, 10.4223 (∼7 s)
ZVDD	1.7141, 10.4323 (∼5 s)	1.7130, 10.4209 (∼10 s)

Euler–Bernoulli beam theory. Input shaping was used with a proportional-derivative controller to slew the flexible beam in order to minimize the induced vibration during the maneuver. The residual vibration due to parameter uncertainty was suppressed by the PZT actuator and the proposed multimode adaptive PPF. An adaptation law based on the recursive least-squares method was developed to update the system's first two natural frequencies. These frequencies were then used by the multimode PPF controller to suppress the residual vibrations. Simulations were run through which the combination of input shaping with the multimode adaptive PPF control clearly offers advantages in the vibration suppression over either of these control methods alone, particularly for systems where there are frequency uncertainties.

References

[1] Dwivedy, S. K., and Eberhard, P., "Dynamic Analysis of Flexible Manipulator, a Literature Review," *Mechanism and Machine Theory*, Vol. 41, No. 7, 2006, pp. 749–777. doi:10.1016/j.mechmachtheory.2006.01.014

[2] Sasiadek, J. Z., and Srinivasan, R., "Dynamic Modeling and Adaptive Control of a Single-Link Flexible Manipulator," *Journal of Guidance, Control, and Dynamics*, Vol. 12, No. 6, 1989, pp. 838–844. doi:10.2514/3.20489

[3] Jnifene, A., and Andrews, W., "Fuzzy Logic Control of the End-Point Vibration in an Experimental Flexible Beam," *Journal of Vibration and Control*, Vol. 10, No. 4, 2004, pp. 493–506. doi:10.1177/1077546304036229

[4] Meressi, T., and Paden, B., "Gain Scheduled H-Infinity Controllers for a Two Link Flexible Manipulator," *Journal of Guidance, Control, and Dynamics*, Vol. 17, No. 3, 1994, pp. 537–543. doi:10.2514/3.21231

[5] Albassam, B. A., "Optimal Near-Minimum-Time Control Design for Flexible Structures," *Journal of Guidance, Control, and Dynamics*, Vol. 25, No. 4, 2002, pp. 618–625. doi:10.2514/2.4945

[6] Goh, C. J., and Caughey, T. K., "On the Stability Problem Caused by Finite Actuator Dynamics in the Collocated Control of Large Space Structure," *International Journal of Control*, Vol. 41, No. 3, 1985, pp. 787–802. doi:10.1080/00207185089611163

[7] Song, G., Schmidt, S. P., and Agrawal, B. N., "Experimental Robustness Study of Positive Position Feedback Control for Active Vibration Suppression," *Journal of Guidance, Control, and Dynamics*, Vol. 25, No. 1, 2002, pp. 179–182. doi:10.2514/2.4865

[8] Fanson, J. L., "An Experimental Investigation of Vibration Suppression in Large Space Structures Using Positive Position Feedback," Ph.D. Thesis, California Inst. of Technology, Pasadena, CA, Nov. 1986.

[9] Meyer, J. L., Harrington, W. B., Agrawal, B. N., and Song, G., "Vibration Suppression of a Spacecraft Flexible Appendage Using Smart Material," *Smart Materials and Structures*, Vol. 7, No. 1, 1998, pp. 95–104. doi:10.1088/0964-1726/7/1/011

[10] Shan, J. J., Liu, H. T., and Sun, D., "Slewing and Vibration Control of a Single-Link Flexible Manipulator by Positive Position Feedback (PPF)," *Mechatronics*, Vol. 15, No. 4, 2005, pp. 487–503. doi:10.1016/j.mechatronics.2004.10.003

[11] Preumont, A., *Vibration Control of Active Structures: An Introduction*, Kluwer Academic, Norwell, MA, 2007, pp. 101–103.

[12] Singer, N. C., and Seering, W. P., "Preshaping Command Inputs to Reduce System Vibration," *Journal of Dynamic Systems, Measurement and Control*, Vol. 112, No. 1, 1990, pp. 76–82. doi:10.1115/1.2894142

[13] Smith, O. J. M., "Posicast Control of Damped Oscillatory Systems," *Proceedings of the IRE*, Vol. 45, No. 9, 1957, pp. 1249–1255. doi:10.1109/JRPROC.1957.278530

[14] Singhose, W., "Command Shaping for Flexible Systems: A Review of the First 50 Years," *International Journal of Precision Engineering and Manufacturing*, Vol. 10, No. 4, 2009, pp. 153–168. doi:10.1007/s12541-009-0084-2

[15] Banerjee, A. K., "Dynamics and Control of the WISP Shuttle-Antennae System," *Journal of Astronautical Sciences*, Vol. 41, No. 1, 1993, pp. 73–90.

[16] Magee, D., and Book, W. J., "Filtering Schilling Manipulator Commands to Prevent Flexible Structure Vibration," *Proceedings of the American Control Conference*, Baltimore, MD, 1994.

[17] Singhose, W., Eloundou, R., and Lawrence, J., "Command Generation for Flexible Systems by Input Shaping and Command Smoothing," *Journal of Guidance, Control, and Dynamics*, Vol. 33, No. 6, 2010, pp. 1697–1707. doi:10.2514/1.50270

[18] Khorrami, F., Jain, S., and Tzes, A., "Experimental Results on Adaptive Nonlinear Control and Input Preshaping for Multilink Flexible Manipulators," *Automatica*, Vol. 31, No. 1, 1995, pp. 83–97. doi:10.1016/0005-1098(94)00070-Y

[19] Banerjee, A. K., and Singhose, W., "Command Shaping in Tracking Control of a Two-Link Flexible Robot," *Journal of Guidance, Control, and Dynamics*, Vol. 21, No. 6, 1998, pp. 1012–1015. doi:10.2514/2.4343

[20] Tuttle, T. D., and Seering, W. P., "Vibration Reduction in 0-G Using Input Shaping on the MIT Middeck Active Control Experiment," *Proceedings of the American Control Conference*, Seattle, WA, 1995.

[21] Singhose, W., Bohlke, K., and Seering, W. P., "Fuel-Efficient Pulse Command Profiles for Flexible Spacecraft," *Journal of Guidance, Control, and Dynamics*, Vol. 19, No. 4, 1996, pp. 954–960. doi:10.2514/3.21724

[22] Singhose, W., Derezinski, S., and Singer, N., "Extra-Insensitive Input Shapers for Controlling Flexible Spacecraft," *Journal of Guidance, Control, and Dynamics*, Vol. 19, No. 2, 1996, pp. 385–391. doi:10.2514/3.21630

[23] Tuttle, T. D., and Seering, W. P., "Experimental Verification of Vibration Reduction in Flexible Spacecraft Using Input Shaping," *Journal of Guidance, Control, and Dynamics*, Vol. 20, No. 4, 1997, pp. 658–664. doi:10.2514/2.4128

[24] Gorinevsky, D., and Vukovich, G., "Nonlinear Input Shaping Control of Flexible Spacecraft Reorientation Maneuver," *Journal of Guidance, Control, and Dynamics*, Vol. 21, No. 2, 1998, pp. 264–270. doi:10.2514/2.4252

[25] Hu, Q., and Ma, G., "Vibration Suppression of Flexible Spacecraft During Attitude Maneuvers," *Journal of Guidance, Control, and Dynamics*, Vol. 28, No. 2, 2005, pp. 377–380. doi:10.2514/1.12967

[26] Singhose, W., Biediger, E., Okada, H., and Matunaga, S., "Closed-Form Specified-Fuel Commands for On-Off Thrusters," *Journal of Guidance, Control, and Dynamics*, Vol. 29, No. 3, 2006, pp. 606–611. doi:10.2514/1.15340

[27] Singhose, W. E., Seering, W. P., and Singer, N. C., "Input Shaping for Vibration Reduction with Specified Insensitivity to Modeling Errors," *Proceedings of the Japan/USA Symposium on Flexible Automation*, Boston, MA, 1996, pp. 307–313.

[28] Singhose, W. E., Porter, L. J., and Singer, N. C., "Vibration Reduction Using Multihump Extra-Insensitive Input Shapers," *Proceedings of the American Control Conference*, Seattle, WA, 1995.

[29] Kojima, H., and Singhose, W., "Adaptive Deflection-Limiting Control for Slewing Flexible Space Structures," *Journal of Guidance, Control, and Dynamics*, Vol. 30, No. 1, 2007, pp. 61–67. doi:10.2514/1.23668

[30] Tzes, A., and Yurkovich, S., "An Adaptive Input Shaping Control Scheme for Vibration Suppression in Slewing Flexible Structures," *IEEE Transactions on Control Systems Technology*, Vol. 1, No. 2, 1993, pp. 114–121. doi:10.1109/87.238404

[31] Bodson, M., "An Adaptive Algorithm for the Tuning of Two Input Shaping Methods," *Automatica*, Vol. 34, No. 6, 1998, pp. 771–776. doi:10.1016/S0005-1098(98)00004-1

[32] Kwak, M. K., Heo, S., and Jin, G. J., "Adaptive Positive Position Feedback Controller Design for the Vibration Suppression of Smart Structures," *Smart Structures and Materials 2002: Modeling, Signal Processing, and Control*, Society of Photo-Optical Instrumentation Engineers, Bellingham, WA, 2002, pp. 246–255.

[33] Baz, A., and Hone, J. T., "Adaptive Control of Flexible Structures Using Modal Positive Position Feedback," *International Journal of Adaptive Control and Signal Processing*, Vol. 11, No. 3, 1997, pp. 231–253. doi:10.1002/(SICI)1099-1115(199705)11:3<231::AID-ACS435>3.0.CO;2-8

[34] Rew, K., Han, J., and Lee, I., "Multi-Modal Vibration Control Using Adaptive Positive Position Feedback," *Journal of Intelligent Material Systems and Structures*, Vol. 13, No. 1, 2002, pp. 13–22. doi:10.1177/1045389X02013001866

[35] Junkins, J. L., and Kim, Y., *Introduction to Dynamics and Control of Flexible Structures*, AIAA, Washington, D.C., 1993, pp. 197–213.

[36] Bandyopadhyay, B., Manjunath, T., and Umapathy, M., *Modeling,*

Control and Implementation of Smart Structures: A FEM–State-Space Approach, Springer–Verlag, Berlin, 2007, pp. 23–44.

[37] Moheimani, S. O. R., and Fleming, A. J., *Piezoelectric Transducers for Vibration Control and Damping*, Springer–Verlag, London, 2006, pp. 9–26.

[38] Inman, D. J., *Vibration with Control*, Wiley, West Sussex, England, U.K., 2006, pp. 57–71.

[39] Mohamed, Z., and Tokhi, M. O., "Command Shaping Techniques for Vibration Control of a Flexible Robot Manipulator," *Mechatronics*, Vol. 14, No. 1, 2004, pp. 69–90. doi:10.1016/S0957-4158(03)00013-8

[40] Ioannou, P., and Fidan, B., *Adaptive Control Tutorial*, Society for Industrial and Applied Mathematics, Philadelphia, 2006, pp. 13–48.